

Computational Determination of Potential Inhibitors of SARS-CoV-2 Main Protease

Son Tung Ngo,^{ab*} Ngoc Quynh Anh Pham,^c Ly Le,^d Duc-Hung Pham,^{e*} and Van V. Vu,^{f*}

^aLaboratory of Theoretical and Computational Biophysics, Ton Duc Thang University, Ho Chi Minh City 700000, Vietnam

^bFaculty of Applied Sciences, Ton Duc Thang University, Ho Chi Minh City 700000, Vietnam

^cFaculty of Chemical Engineering, Ho Chi Minh City University of Technology (HCMUT), Ho Chi Minh City 700000, Vietnam

^dSchool of Biotechnology, International University, Ho Chi Minh City 700000, Vietnam

^eDivision of Gastroenterology, Hepatology and Nutrition Cincinnati Children's Hospital Medical Center, Cincinnati 45229, OH, USA

^fNTT Hi-Tech Institute, Nguyen Tat Thanh University, Ho Chi Minh City 700000, Vietnam

ABSTRACT: The novel coronavirus (SARS-CoV-2) has infected over 850,000 people and caused more than 42000 deaths worldwide as of April 1st, 2020. As the disease is spreading rapidly all over the world, it is urgent to find effective drugs to treat the virus. The main protease (Mpro) of SARS-CoV-2 is one of the potential drug targets. In this work, we used rigorous computational methods, including molecular docking, fast pulling of ligand (FPL), and free energy perturbation (FEP), to investigate potential inhibitors of SARS-CoV-2 Mpro. We first tested our approach with three reported inhibitors of SARS-CoV-2 Mpro; and our computational results are in good agreement with the respective experimental data. Subsequently, we applied our approach on a databases of ~4600 natural compounds found in Vietnamese plants, as well as 8 available HIV-1 protease (PR) inhibitors and an aza-peptide epoxide. Molecular docking resulted in a short list of

35 natural compounds, which was subsequently refined using the FPL scheme. FPL simulations resulted in five potential inhibitors, including 3 natural compounds and two available HIV-1 PR inhibitors. Finally, FEP, the most accurate and precise method, was used to determine the absolute binding free energy of these five compounds. FEP results indicate that two natural compounds, *cannabisin A* and *isoacteoside*, and an HIV-1 PR inhibitor, *darunavir*, exhibit large binding free energy to SARS-CoV-2 Mpro, which is larger than that of **13b**, the most reliable SARS-CoV-2 Mpro inhibitor recently reported. The binding free energy largely arises from van der Waals (vdW) interaction. We also found that Glu166 form H-bonds to all the inhibitors. Replacing Glu166 by an alanine residue leads to ~ 2.0 kcal/mol decreases in the affinity of *darunavir* to SARS-CoV-2 Mpro. Our results could contribute to the development of potentials drugs inhibiting SARS-CoV-2.

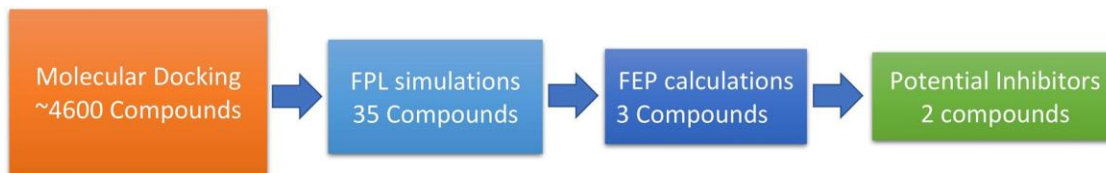
INTRODUCTION

Members of the Coronaviridae virus family often cause mild respiratory syndrome in humans.¹ However, the severe acute respiratory syndrome coronavirus (SARS-CoV) and the Middle East respiratory syndrome coronavirus (MERS-CoV) are transfected from animals to human and cause severe cases of respiratory syndromes and deaths.²⁻³ In 2002, SARS-CoV was first recorded in Guangdong, China, and linked to 8096 laboratory-confirmed cases of infection and 774 deaths.³ The natural reservoir of SARS-CoV is Chinese horseshoe bats⁴ and intermediate hosts are civet cats and raccoon dogs.⁵ This shows that Coronavirus can induce severe symptoms and potential pneumonia and death. In December 2019, a novel coronavirus (2019-nCoV or SARS-CoV-2) that has similar sequence to SARS-CoV emerged in Wuhan, Hubei province, China.⁶⁻⁸ The initial cluster of infection seemed to relate to Huanan seafood market and SARS-CoV-2 is thought to originate from bat though the intermediate hosts are still unknown;⁹ human-to-human transmission has been confirmed.¹⁰ As of April 1st, 2020, SARS-CoV-2 has infected more than 850,000 people and caused over 42,000 deaths worldwide.¹¹

Coronaviruses have the largest genomes among all known RNA virus, ranging from 26 – 32 kb in length, which encode structural and non-structural proteins.¹²⁻¹³ SARS-CoV-2 genome encodes more than 20 proteins, which include the main protease (Mpro), a 3C-like protease (3CLP) that shares 96,1% similarity with 3CLP of SARS-CoV.¹³⁻¹⁴ Mpro, a homodimeric cysteine protease, plays an important role in SARS virus replication and transcription. When the messenger RNA of the virus is translated polyproteins, Mpro is first auto-cleaved to become a mature enzyme, which in turn cleaves all the 11 remaining downstream non-structural proteins of the polyproteins to polypeptides, which are required for the replication process of the virus.¹³ SARS-CoV Mpro has

thus been an attractive drug target.¹⁴⁻¹⁵ Darunavir and ritonavir can potentially inhibit SARS-CoV-2 Mpro and have been put into clinical trials for Covid19 treatment.¹⁶⁻¹⁷

Computer-aided drug design (CADD) is frequently used to estimate the probable inhibitors that could prevent the activity of an enzyme. This method significantly decreases the time and cost to develop a new drug.¹⁸ Determination of the ligand-binding free energy is one of the most critical factors in CADD.¹⁹ Many schemes were then developed to resolve this problem.²⁰ Typically, the ligand-binding affinity of several thousand ligands to a protein is frequently predicted via the molecular docking method.²¹ ; shortlist of these compounds would be then refined via more computationally expensive binding free energy methods such as the molecular mechanism/Poisson-Boltzmann surface area (MM/PBSA),²²⁻²⁴ linear interaction energy (LIE),²⁵⁻²⁶ or fast pulling of ligand (FPL)²⁷ approaches. The top-lead potential inhibitors will be finally validated through an accurate binding free energy approach such as the free energy perturbation (FEP),²⁸⁻²⁹ thermodynamic integration (TI),³⁰⁻³¹ and non-equilibrium molecular dynamics simulations (NEMD).³² Especially, in some cases, calculations required higher accuracy and precision can be conducted via a combination of temperature/Hamiltonian replica exchange molecular dynamics (REMD) simulations and perturbation method.³³⁻³⁶ In this work, we carried out computational investigations according to Scheme 1 to evaluate the potential inhibitors for SARS-CoV-2 Mpro. The obtained results could help enhance the development of SARS-CoV-2 therapy.



Scheme 1. Computational strategy to determine the probable natural inhibitors of SARS-CoV-2 Mpro.

MATERIALS & METHODS

Structure and Parameter of Complexes

Three-dimensional structures of SARS-CoV-2 Mpro was downloaded from <https://innophore.com/>.³⁷ It should be noted that the modelled structure is in good agreement with the recent experiment (Figure S1 of SI1 file).³⁸ SARS-CoV-2 Mpro was parameterized using Amber99SB-ILDN force field.³⁹ Ligand structures were downloaded from PubChem database.⁴⁰ The ligands were parameterized with general Amber force field (GAFF)⁴¹ using the combination of AmberTools18⁴² and ACPYPE⁴³ protocols. The atomic charges were allocated via the Restrained Electrostatic Potential (RESP) method⁴⁴ computed with quantum chemical calculation at B3LYP double-hybrid functional in combination with 6-31G(d,p) basis set. In addition, the SARS-CoV-2 Mpro is mutated via PyMOL mutagenesis tools.⁴⁵

Molecular Docking Simulations

The molecular docking using the Autodock Vina package⁴⁶ was employed to rapidly determine the ligand binding pose and affinity to SARS-CoV-2 Mpro with the exhaustiveness of 8 referring to the previous study.⁴⁷ The best docking mode was selected as the lowest obtained binding energy results. The grid center was selected as the center of mass of aza-peptide epoxide, which bound to the active site of SARS-CoV Mpro.⁴⁸ The grid size was chosen as $26 \times 26 \times 26$ Angstrom.

Molecular Dynamics Simulations

GROMACS version 5.1.5⁴⁹ was employed to simulate the structural change of the solvated complex SARS-CoV-2 Mpro + inhibitor. The parameters for MD simulations were referred to the

previous works.⁵⁰ The time steps of MD simulations were set to 2 fs. The electrostatic interaction was mimicked via fast smooth Particle-Mesh Ewald electrostatics method.⁵¹ The cut-off of the van der Waals interaction was picked as 0.9 nm. The solvated complex was minimized using the steepest descent method. The energy minimized system was relaxed over 100 ps of NVT and 2 ns of NPT ensembles at 310 K. During the NVT and NPT simulations, C_{α} atoms of the SARS-CoV-2 Mpro was softly retrained using a harmonic force. The coordinates of the solvated complexes were monitored over the atomistic simulations every 10 ps.

Free Energy Calculation

Fast pulling of ligand (FPL) approach. The last snapshot of NPT simulations was used as the initial structure for SMD simulation.²⁷ Details of the computations were referred to the previous studies.²⁷ In particular, the (x, y, z) dimensions of the systems are (9.83, 5.92, 8.70) nm as shown in **Figure 1**. The systems in FPL simulations consists of 1 SARS-CoV-2 Mpro, 1 ligand, 15 000 water molecules, and Na^+ ions for a total of ca. 50 000 atoms. The pulling speed (v) and spring constant cantilever (k) were set at 0.005 nm ps^{-1} and $600 \text{ kJ mol}^{-1} \text{ nm}^{-2}$, respectively. During the simulations, the C_{α} atoms of Mpro were positionally restrained using a weak harmonic potential. A harmonic force was put on the center of mass of the inhibitor to disassociate it from the binding cavity of the SARS-CoV-2 Mpro (**Figure 1**). The pulling force value and displacement of ligand along unbinding direction were monitored every 0.1 ps. The FPL simulations were repeated with 8 independent trajectories to guarantee the sampling of simulations.

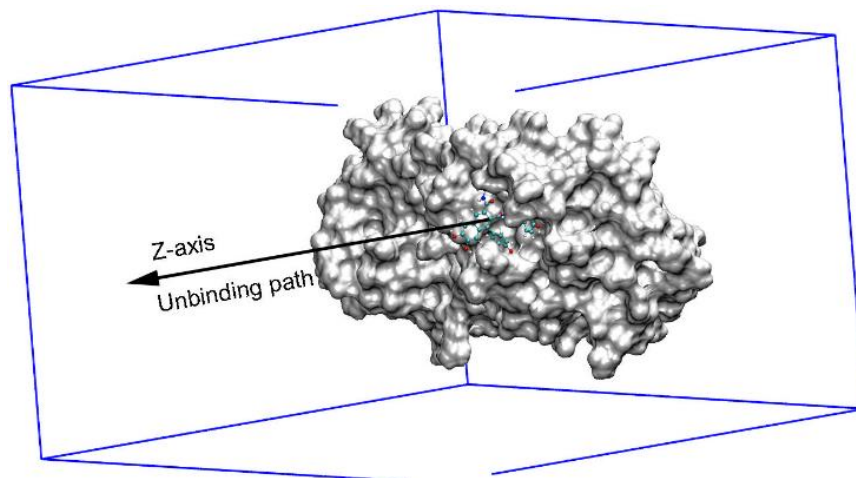


Figure 1. The computational model for FPL simulations of SARS-CoV-2 Mpro - ligand binding affinity.

Free energy perturbation (FEP) simulations.⁵² The last snapshot of NPT simulations was used as the initial conformation for 20 ns-long MD simulations. In particular, the SARS-CoV-2 Mpro + inhibitor complex was inserted into a dodecahedron periodic boundary condition (PBC) box with a volume of ca. 820 nm³. The complexed system comprises 1 SARS-CoV-2 Mpro, 1 ligand, 25 280 water molecules, and 4 Na⁺ ions for a total of ca. 80 600 atoms. Moreover, the isolated inhibitor was inserted into a dodecahedron PBC box with a volume of ca. 85 nm³. The solvated ligand system consists of 1 ligand and ca. 2750 water molecules for a total of ca. 8 300 atoms. The equilibrium conformation of MD simulations was then employed as the starting structure for FEP calculations according to the previous study.⁵⁰ During FEP simulations, the coupling parameter λ , varies from 0 to 1, was employed to evaluate the free energy change ΔG of the system modification from the *full-interaction* state ($\lambda = 0$) to the *non-interaction* state ($\lambda = 1$) via the alteration of the systemic Hamiltonian between various circumstances. The change of a ligand from *full-interaction* to *non-interaction* states with surrounding molecules is called the ligand annihilation process (**Figure 2**). Eight values of λ_{cou} , including 0.00, 0.100, 0.20, 0.35, 0.50, 0.65, 0.80, and 1.00, were

used to modify the Coulomb interactions. Nine values of λ_{vdW} , including 0.00 0.10 0.25 0.35 0.50 0.65 0.75 0.90 1.00, to alter the van der Waals (vdW) interactions. Sixteen alter- λ simulations were performed to demolish a ligand from a solvated system (**Figure 2**). The total energy change of the ligand annihilation process was then summed via the Bennet's acceptance ratio (BAR) method.⁵³ Finally, the absolute binding free energy between a ligand to SARS-CoV-2 Mpro was deduced as the different energy between two annihilation processes involving decoupling the ligand from the solvated ligand system and from the solvated protein-ligand system.

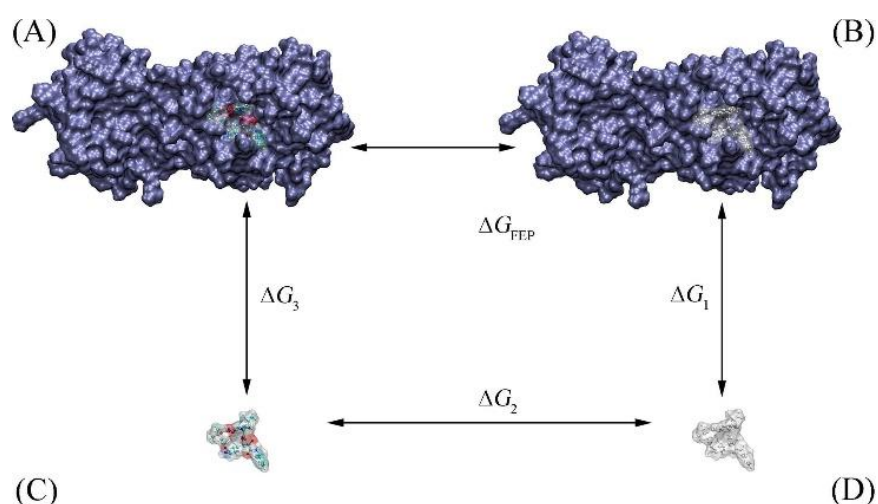


Figure 2. Thermodynamics diagram of determination of the absolute binding free energy between a ligand and SARS-CoV-2 Mpro. A) The full-interaction state of a ligand with surrounding molecules, including the protease and solvent molecules. B) A dummy ligand with the solvated protease. C) The full-interaction state of a ligand with the solvent molecules. D) A dummy ligand in solution. A dummy ligand is a ligand that has no non-bonded interaction with neighboring molecules. The solvent molecules are hidden for clarity.

Structural Analysis

A hydrogen bond (HB) is determined when an acceptor (A)-hydrogen (H)-donor (D) angle is larger than 135° and the A - D distance is less than 0.35 nm. The two-dimensional interaction diagram between a protein and a ligand was generated using the LigPlot++ program.⁵⁴ Moreover, pharmacokinetics of the top-lead compounds were predicted using the PreADME server.⁵⁵

RESULTS AND DISCUSSION

Potential Inhibitor Screening using Molecular Docking

Autodock Vina⁴⁶ is one of the most popular free packages to roughly and rapidly estimate the binding affinity and binding pose of a ligand to a protein. The successful-docking rate of the package was up to 81 % according to our previous benchmark study on over 800 protein-ligand complexes.⁴⁷ We used Autodock Vina to dock three previously reported ligands³⁸ to SARS-CoV-2 Mpro and obtained binding energies reasonably consistent to experimentally determined values (**Table 1**). Therefore, in this project, Autodock Vina⁴⁶ was employed to rapidly evaluate the binding affinity of ca. 4600 natural compounds from the Vietherb database.⁵⁶ Because some current HIV-1 PR inhibitors, such as darunavir¹⁶ or ritonavir,¹⁷ have been tested for SARS-CoV-2 inhibition, eight drugs inhibiting HIV-1 PR, including amprenavir, atazanavir, darunavir, indinavir, lopinavir, nelfinavir, ritonavir, and saquinavir, were also investigated. Moreover, the binding of aza peptide epoxide was also redocked to SARS-CoV-2 Mpro in order to compare with other ligands. The binding affinity of top-lead and all compounds to SARS-CoV-2 Mpro is provided in Table S1 of the Supporting Information 1 (SI1) and Supporting Information 2 (SI2) files, respectively. The obtained docking energies fall the range from -1.2 to -9.8 kcal/mol with the median of -6.22 ± 0.02 kcal/mol (the computed error is the standard error of the mean) (**Figure 3**).

Table 1. Recently reported inhibitors of SARS-CoV-2 Mpro

N ⁰	Compound Name	$\Delta G_{\text{Dock}}^{\text{a}}$	$\Delta G_{\text{EXP}}^{\text{b}}$
1	11r	-7.1	-9.23
2	13a	-6.7	-7.70
3	13b	-6.9	-8.45

^aDocking binding free energy obtained by Autodock Vina.⁴⁶ ^bExperimental binding free energy ΔG_{EXP} roughly estimated based on IC50 value reported recently,³⁸ assuming that inhibition constant (k_i) is equal to IC50 value. The unit of ΔG is kCal/mol.

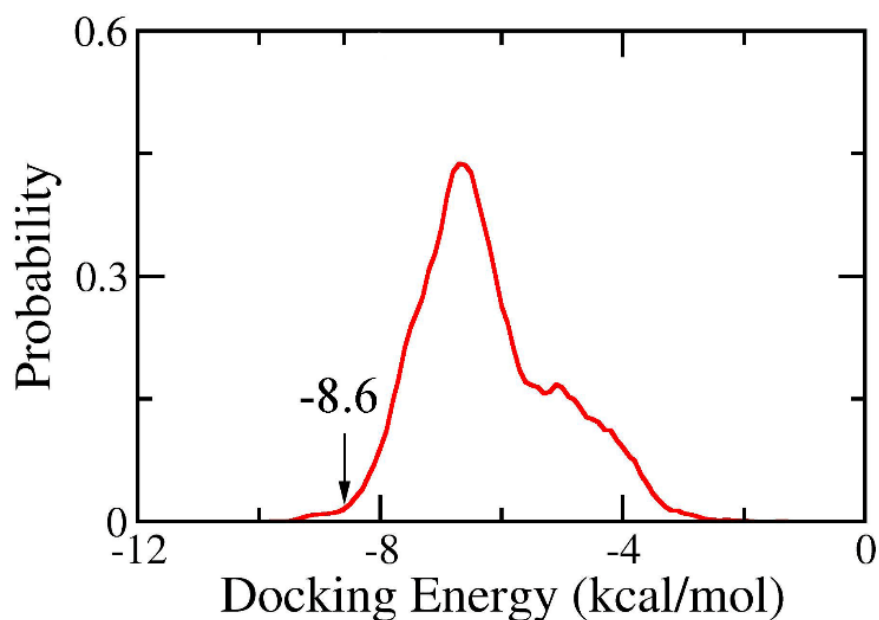


Figure 3. Distribution of docking energy between 4663 natural compounds and SARS-CoV-2 Mpro.

There are 35 natural compounds from the Vietherb database exhibiting large ligand affinity to SARS-CoV-2 Mpro. The affinity of these compound ranges from -8.6 to -9.8 kcal/mol (Table S1 in SI1), which is significantly larger than that found in the range of -6.4 to -7.6 kcal/mol for the 8 HIV-1 PR inhibitors, and aza peptide epoxide. The 35 natural compounds form more HBs to SARS-CoV-2 Mpro than these 9 compounds (**Figure 4** and Table S3 of SI2).

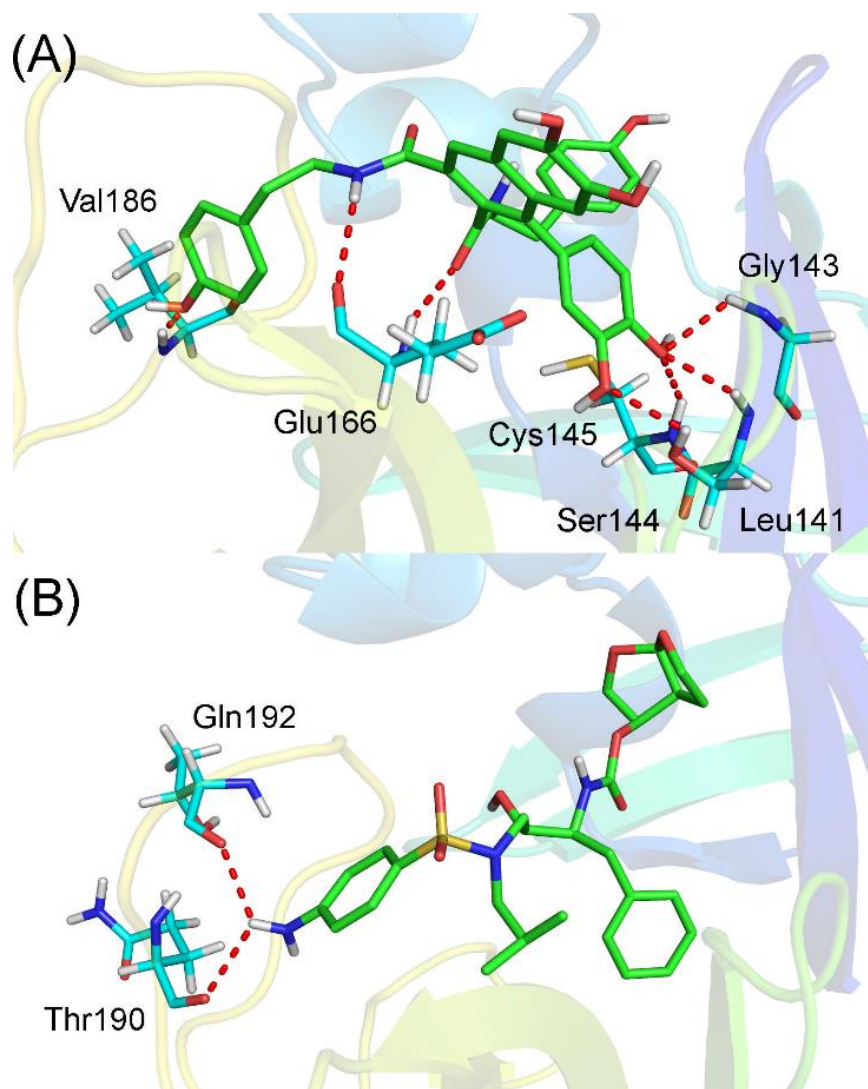


Figure 4. Docked conformations of SARS-CoV-2 Mpro + *cannabisin A* (A) and SARS-CoV-2 Mpro + *darunavir* (B) complexes.

Refining Docking Results using FPL Simulations

The obtained docking results were refined using the FPL method.²⁷ The FPL scheme is a very efficient technique to rapidly explore the binding affinity of a ligand to a protein, when the protein binding cavity accessible to the exogenous ligand without sizable conformational change during the binding/unbinding process. The FPL approach requires a small amount of computing resource, but it could provide results with high accuracy and precision.²⁷ The maximum pulling

force (F_{max}), called rupture force, and the recorded pulling work (W) were used as a criterion to rank the ligand-affinity.^{27, 57} However, as mentioned in the previous work,²⁷ the pulling work is more appropriate than the rupture force as it directly associates with the ligand-binding free energy via isobaric-isothermal Jarzynski equality.⁵⁸⁻⁵⁹

In this work, we carried out FPL simulations to rank the affinity to SARS-CoV-2 Mpro of 44 compounds screened with docking studies. The FPL calculations for **11r**, **13a**, and **13b**³⁸ were also carried out for comparison. The equilibrated snapshot obtaining from 2 ns of NPT simulations was used as an initial structure for the FPL simulations. The maximum pulling force, called rupture force, and pulling work were obtained from 8 independent trajectories. The obtained results are provided in **Table 2**. The mean of recorded rupture forces F_{max} ranges from 416.9 ± 35.4 to 901.0 ± 59.2 pN. The time-dependent pulling forces of these 47 systems are provided in Figure S3 of the SI1. The form of pulling force curves are in good agreement with the previous studies,²⁷ in which the pulling forces continuously increase to maximum values before rapidly dropping to zero after the nonbonded contacts between the ligand to the protein were terminated. Here, the pulling work was selected as a criterion to rank the ligand-affinity (**Figure 5**). The average pulling work W ranges from 36.1 ± 4.5 to 104.0 ± 5.6 kcal/mol (**Table 2**). The FPL-derived pulling work for **11r**, **13a**, **13b** is 43.3 ± 3.9 , 94.6 ± 5.0 , and 91.9 ± 3.6 kcal/mol, respectively, which is consistent with respective experiments.³⁸ This result supports our approach in using FPL to refine the docking results.

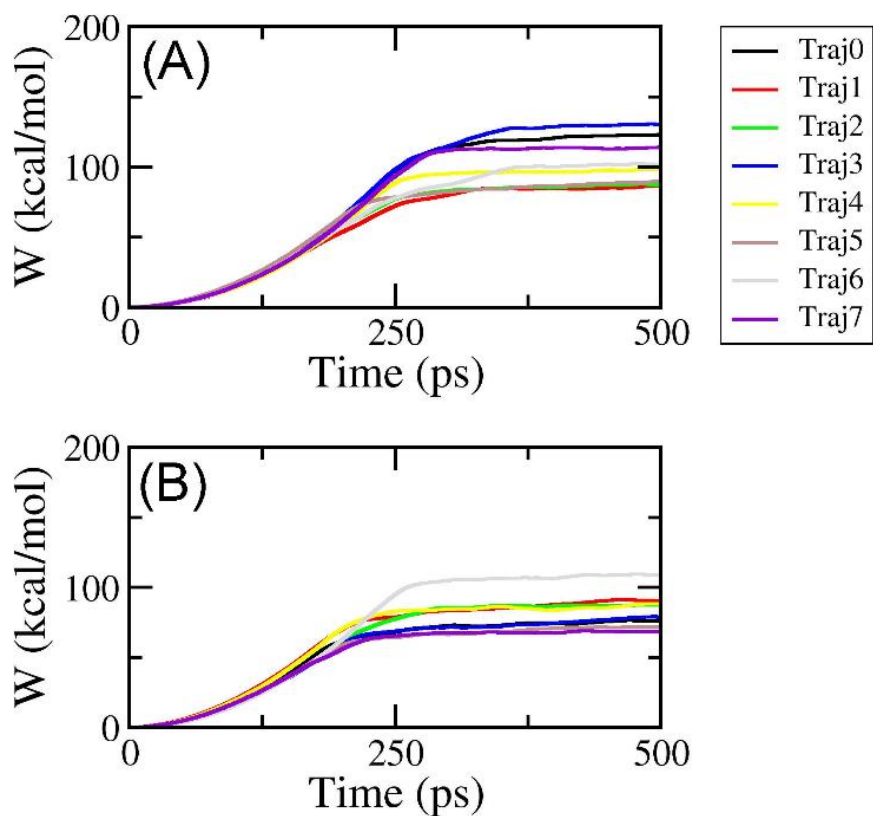


Figure 5. Recorded pulling works during FPL simulations of SARS-CoV-2 Mpro + *cannabisin* A (A) and SARS-CoV-2 Mpro + *darunavir* (B) complexes.

Table 2. FPL results of top-lead compounds screened with molecular docking

N ⁰	Pubchem	Compound Name	ΔF_{Max}^a	W^b	ΔG_{EXP}^c
1		11r	857.5 ± 38.7	94.6 ± 5.0	-9.23
2		13a	496.0 ± 32.5	43.3 ± 3.9	-7.70
3		13b	884.3 ± 36.5	91.9 ± 3.6	-8.45
4	10621	Hesperidin	575.6 ± 46.2	62.7 ± 4.6	
5	73330	Strictinin	633.2 ± 27	67.9 ± 3.8	
6	83489	Eriocitrin	588.7 ± 26.8	71.0 ± 4.8	
7	114777	CHEMBL346119	721.2 ± 38.1	72.6 ± 4.5	
8	122738	Procyanidin B2	668.8 ± 20	77.8 ± 3.7	
9	124356	Physalin F	614.2 ± 23.5	52.6 ± 1.8	
10	156766	Kihadanin B	500.3 ± 30.2	45.0 ± 3.0	
11	179651	Limonin	516.3 ± 31.9	45.1 ± 1.8	
12	183905	6,8-Di-C-Beta-D-Arabinopyranosyl Apigenin	672.6 ± 38.9	67.4 ± 4.8	
13	190799	Stephasubine	807.4 ± 54.4	78.4 ± 7.3	
14	196583	Mulberrofurin G	674.2 ± 52.4	71.7 ± 4.9	

15	442431	Narirutin	535.8 ± 45.3	54.4 ± 5.1
16	480819	Albanol B	546.6 ± 27.7	49.7 ± 3.8
17	5281600	Amentoflavone	710.6 ± 50.9	74.3 ± 6.3
18	5281613	Diosmin	714.0 ± 47.5	77.5 ± 5.6
19	5281627	Hinokiflavone	645.1 ± 51.0	67.6 ± 4.2
20	5317025	Linarin	548.3 ± 21.9	58.5 ± 3.0
21	5319276	Marchantin K	567.6 ± 13.3	50.0 ± 1.7
22	5319278	Marchantin L	616.1 ± 34.0	53.9 ± 3.2
23	5319933	Mulberrofuran Q	539.4 ± 16.4	54.2 ± 2.7
24	5458744	Physalin B 5,6-Epoxyde	476.2 ± 32.9	38.4 ± 3.3
25	6476333	Isoacteoside	730.7 ± 40.1	92.2 ± 4.4
26	6711179	Hypopistephanine	707.0 ± 34.5	65.1 ± 3.8
27	9851181	Isorhoifolin	567.7 ± 36.7	57.9 ± 4.8
28	10456516	Cinchonain-Ib	547.3 ± 33.7	53.5 ± 3.1
29	10461109	Luteolin-7-O-Beta-Rutinoside	608.1 ± 63.0	65.0 ± 6.0
30	11827970	Diosgenin Glucoside	514.8 ± 41.2	49.1 ± 5.6
31	15086398	Cannabisin A	901.0 ± 59.3	104 ± 5.6
32	16760075	Didymin	574.5 ± 50.9	63.7 ± 6.0
33	21123844	Gamma-Chaconine	416.9 ± 35.4	36.1 ± 4.5
34	44558930	Anabsinthin	589.3 ± 57.8	56.4 ± 5.4
35	71437113	2,3-Dihydrohinokiflavone	546.5 ± 36.1	61.5 ± 3.3
36	71448965	Cannabisin D	733.1 ± 32.9	70.4 ± 4.1
37	90473381	N/A	564.9 ± 53.0	50.0 ± 7.1
38	101764560	Quercetin-7-O-Rutinoside	737.9 ± 47.8	79.4 ± 6.4
39	65016	Amprenavir	607.6 ± 29.9	55.4 ± 3.7
40	148192	Atazanavir	647.7 ± 37.9	74.1 ± 3.3
41		Aza-Peptide Epoxyde	586.4 ± 48.2	61.5 ± 6.4
42	213039	Darunavir	817.8 ± 32.0	83.9 ± 4.3
43	5362440	Indinavir	456.3 ± 33.0	48.5 ± 1.7
44	92727	Lopinavir	684.8 ± 44.5	71.2 ± 3.9
45	64143	Nelfinavir	607.9 ± 31.5	58.1 ± 3.0
46	392622	Ritonavir	764.8 ± 54.0	85.9 ± 7.8
47	441243	Saquinavir	601.3 ± 41.6	66.4 ± 4.4

^aMean rupture force ΔF_{Max} and ^bMean pulling work W obtained from 8 independent trajectories of SMD simulations.

^bExperimental binding free energy ΔG_{EXP} roughly estimated based on IC50 value reported recently,³⁸ assuming that inhibition constant (k_i) is equal to IC50 value. The error is standard error of the mean. The unit of energy and work is kcal/mol; the unit of force is pN.

A short list of potential inhibitors of SARS-CoV-2 Mpro was obtained and shown in **Table**

1. The pulling work W for *darunavir* and *ritonavir* is 83.9 and 85.9 kcal/mol, respectively, which

is >11% larger than that of the other HIV-1 PR inhibitors (**Table 2**). Previous computational investigations suggested that *lopinavir* was able to prevent SARS-CoV-2 Mpro.¹⁴ However, FPL results show otherwise, which is consistent with the recent clinical research.⁶⁰ Two natural compounds, *cannabisin A* and *isoacteoside*, have larger W values than that of *ritonavir*. *Cannabisin A*, Pubchem ID of 15086398, adopts the largest values of both W and F_{\max} , which are 104.0 kcal/mol and 901.0 pN, respectively. *Isoacteoside*, Pubchem ID of 6476333, has a pulling work W of 92.2 ± 4.4 kcal/mol. Beside these compounds, *quercetin 7-O-Rutinoside* was also included into the list of potential inhibitors for the SARS-CoV-2 Mpro, because it adopts a W of 79.4 ± 6.4 kcal/mol, which is only 5% small than that of *darunavir*. These five compounds adopt an appropriate pulling work W in comparison with that obtained for **13b** (91.9 ± 3.6 kcal/mol), the most reliable SARS-CoV-2 Mpro inhibitor recently reported.³⁸

Validation of FPL Results using FEP Calculations

Accurate and precise determination of the ligand-binding free energy probably reduces drug discovery cost.⁶¹ Therefore, in order to validate the FPL results, the absolute binding free energy between five ligands was computed using FEP method (**Table 3**), one of the most accurate and precise methods known to date.^{20, 62} FEP is often used in CADD as it often provides results consistent with experiments.⁶³⁻⁶⁵ The binding free energy of three recently reported inhibitors of SARS-CoV-2 Mpro, including **11r**, **13a**, and **13b**, was also calculated. The good agreement between computational and experimental values³⁸ indicates that FEP method is reliable in calculating binding free energy of ligands to SARS-CoV-2 Mpro.

Table 4. Computationally determined potential inhibitors for wild type (WT) and E166A mutants SARS-CoV-2 Mpro

N ^o	Pubchem ID	Complex	Herb Name	ΔG_{cou}	ΔG_{vdW}	ΔG_{FEP}^a	ΔG_{EXP}^b
1		WT + 11r		-6.02	-7.30	-13.31 \pm 2.58	-9.23
2		WT + 13a		-0.59	-7.59	-8.18 \pm 2.20	-7.70
3		WT + 13b		-1.97	-7.22	-9.18 \pm 2.48	-8.45
4	101764560	WT + <i>Quercetin 7-O-Rutinoside</i>	<i>Platycodon Grandiflorum</i>	-3.82	-9.33	-5.52 \pm 1.18	
5	15086398	WT + <i>Cannabisin A</i>	<i>Cannabis Sativa</i>	-2.57	-10.20	-12.76 \pm 1.37	
6	6476333	WT + <i>Isoacteoside</i>	<i>Fernandoa Adenophylla</i>	-2.06	-7.34	-9.40 \pm 2.64	
7	213039	WT + <i>Darunavir</i>		-3.44	-8.52	-11.96 \pm 1.99	
8	392622	WT + <i>Ritonavir</i>		2.10	-9.83	-7.73 \pm 1.77	
9	213039	E166A + <i>Darunavir</i>		-1.58	-8.32	-9.90 \pm 2.48	

^aAbsolute binding free energy ΔG_{FEP} obtained using 3 independent FEP calculations. Experimental binding free energy ΔG_{EXP} roughly estimated based on IC50 value reported recently,³⁸ assuming that inhibition constant (k_i) is equal to IC50 value. The error is standard error of the mean values. The unit of energy and work is kcal/mol.

The equilibrium snapshots of the SARS-CoV-2 Mpro + inhibitor systems generated in NPT simulations were treated as the initial conformations for MD simulations. These MD simulations were set to run for 20 ns, in which all-atom RMSD of the complex was recorded every 10 ps (Figure S4 of the SI1). During the MD simulations, the binding pose between the SARS-CoV-2 Mpro and the inhibitor was refined under the effects of the interaction among them. The number of HBs between protein-ligand fluctuates from the beginning of MD simulations and becomes stables after 10 ns of MD simulations (**Figure 6**). It is consistent with all-atom RMSD of the complex over the MD simulations (Figure S4 of the SI1). **Figure 7** shows the dominant structures and binding poses of *cannabisin A* and *darunavir* with SARS-CoV-2 Mpro, respectively. The poses for SARS-CoV-2 Mpro + *isoacteoside*, *quercetin 7-o-rutinoside*, and *ritonavir* complexes are provided in Figure S5-7 of the SI1. Interestingly, Glu166 appears to be an important residue involving in the binding of the inhibitors to SARS-CoV-2 Mpro as it forms HBs with all of these inhibitors. The mutation of Glu166 could possibly alter the affinity of inhibitors to SARS-CoV-2 Mpro.

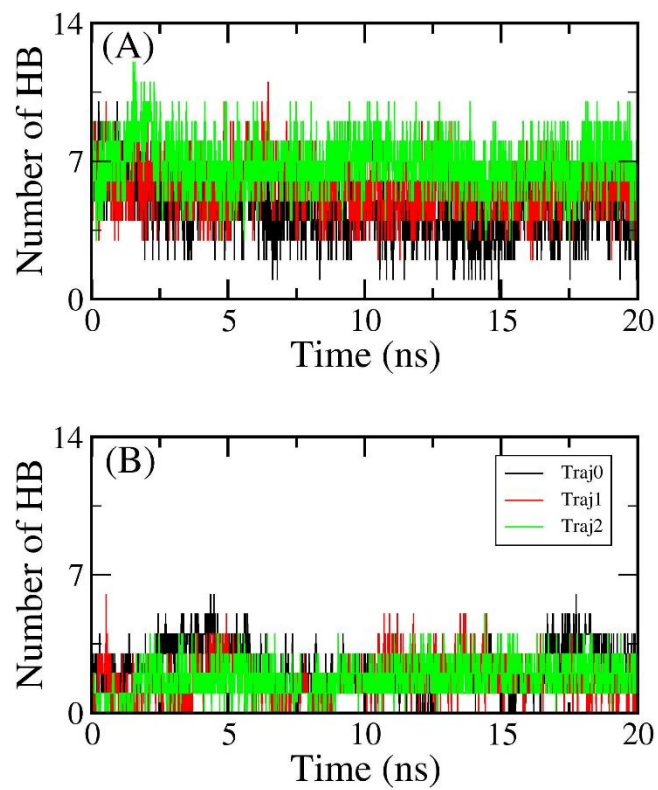


Figure 6. The number of HBs between SARS-CoV-2 Mpro and *cannabisin A* (A) and *darunavir* (B).

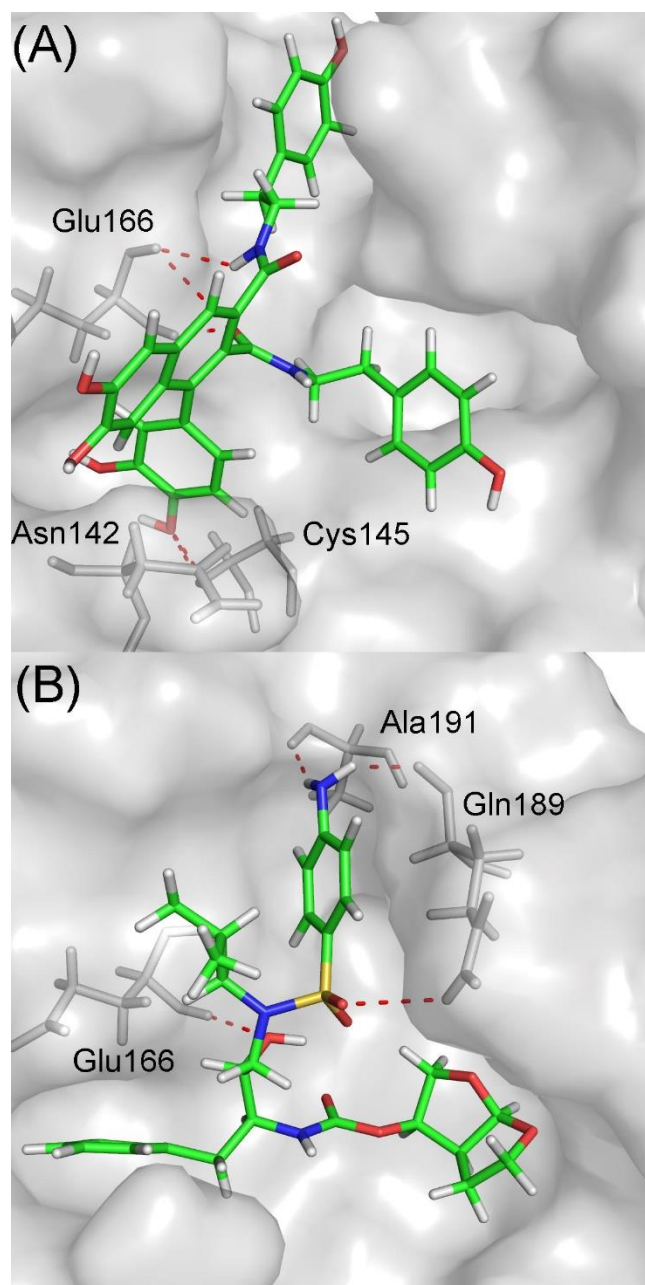


Figure 7. The binding pose of the SARS-CoV-2 Mpro + *cannabisin A* (A) and SARS-CoV-2 Mpro + *darunavir* (B) systems, obtained by all-atom clustering with a cutoff 0.3 nm using 3000 equilibrium snapshots.

The work values of the decoupling ligand from the solvated system are used to determine the free energy change over the annihilation ligand process (**Figure 2**). Sixteen λ -alteration MD simulations length of 2 ns were employed to calculate the work values. The soft-core potentials

were used to characterize the altered Hamiltonian system. However, the soft-core potentials cost much more CPU time than the traditional one. Therefore, the performance of MD simulation is significantly reduced during λ -alteration simulations. Totally, MD simulations were carried out in 219 ns over 3 trajectories. The free energy terms were then computed using the BAR method⁵³ over the interval 1-2 ns of the λ -alteration simulations with a period of 100 ps. Overall, the absolute binding free energy between five potential inhibitors to SARS-CoV-2 Mpro was then obtained (Table 4Error! Reference source not found.).

According to results showing in Table 4Error! Reference source not found., the vdW free energy interaction energy dominates over the electrostatic free interaction energy during a ligand binding to SARS-CoV-2 Mpro. Moreover, *darunavir* adopts a stronger binding free energy (-11.96 ± 1.99 kcal/mol) to SARS-CoV-2 Mpro than *ritonavir* (-7.73 ± 1.77 kcal/mol). This result is consistent with recent clinical research⁶⁰ that *ritonavir* only has weak inhibitory effect on SARS-CoV-2.

Quercetin 7-o-rutinoside, a compound from *platycodon grandiflorum*,⁵⁶ exhibits poor binding affinity SARS-CoV-2 Mpro (-5.52 ± 1.18 kcal/mol). *Isoacteoside*, a compound from *fernandoa adenophylla*,⁵⁶ has an binding affinity of -9.40 ± 2.64 kcal/mol, which falls between that of *ritonavir* and *darunavir*. *Cannabisin A*, a compound from *cannabis sativa*,⁶⁶ adopts the strongest binding affinity to the SARS-CoV-2 Mpro (-12.76 ± 1.37 kcal/mol).

FEP result suggests that *canabisin A*, *isoacetoside*, and *darunavir* are the potential inhibitors for SARS-CoV-2 Mpro since their binding free energies are larger than that of compound **13b**, has a computational binding free energy of -9.18 ± 2.48 kcal/mol (Table 4). In addition, the cell membrane crossing ability was then predicted for these compounds using the preADMET server. The logP values predicted for *Canabisin A* is 5.18, which is similar to that of

ritonavir (5.59) and higher than that of *darunavir* (2.22). Having a logP value similar to an approved drug further supports *canabisin A* as a potential drug for SARS-CoV-2. In addition, the predicted logP value of *isoacetoside* is relatively small but is still on the positive side and should still be included in future study.

Potential Key residue in SARS-CoV-2 Mpro-ligand binding

As mentioned above, residue Glu166 is located in the active site of SARS-CoV-2 Mpro and form HBs to all FEP-calculated inhibitors. The mutation of this residue could possibly alters the binding affinity of a ligand to SARS-CoV-2 Mpro. To test this hypothesis, we have replaced Glu166 with an alanine residue and carried FEP calculation for E166A SARS-CoV-2 Mpro + *darunavir* complex (Table 1). Upon E166A mutation, the calculated binding affinity of *darunavir* to SARS-CoV-2 Mpro changes from -11.96 ± 1.99 kcal/mol to -9.90 ± 2.48 kcal/mol. This ~ 2 kcal/mol decreases in binding affinity mostly arises from the weakening in coulomb interaction (ΔG_{cou}) due to the loss of HBs formed by the residue 166. This result suggest that G166 is potentially a key residue in ligand binding to SARS-CoV-2, and its mutation to hydrophobic residue could lead to decreases in inhibitory effect of ligands.

CONCLUSIONS

In this work, we utilized a rigorous computational approach to determine potential inhibitors of SARS-CoV-2 Mpro. First, we tested our approach on 3 recently reported inhibitors of SARS-CoV-2 Mpro and obtained computational results consistent with the experimental data. Subsequently, we investigated a database of 4600 natural compounds found in Vietnamese plants (Vietherbs). Eight HIV-1 PR inhibitors and an aza-peptide epoxide were added to the database.

The database was first shortlisted to 44 by molecular docking, which was further refined using FPL simulations to 5 compounds. The refined compounds were validated with FEP method, the most accurate binding free energy estimation method. We found that 2 two natural compounds, *cannabisin A* and *isoacteoside*, in the Vietherbs database and an HIV-1 PR inhibitors, *darunavir*, can potentially inhibit SARS-CoV-2 Mpro since their affinities are significantly larger than that of the compound **13b**, a most reliable SARS-CoV-2 inhibitors from the recent work.³⁸ Moreover, the others HIV-1 PR inhibitors are unlikely to prevent SARS-CoV-2 Mpro, consistent with a recent clinical study.⁶⁰ Furthermore, we also found that the residue Glu166 possibly plays an important role in the binding of a ligand to SARS-CoV-2 Mpro, which could be a target for future study.

ASSOCIATED CONTENT

Supporting Information

Supporting Information Available: List of top-lead inhibitors for SARS-CoV-2 Mpro obtained via molecular docking; two-dimensional protein-ligand interaction diagram of top-lead compounds; superposition of modelled and experimental SARS-CoV-2 Mpro; superposition of experimental and docked conformations of the compound **13b**; FPL results; all-atom RMSD of SARS-CoV-2 Mpro + inhibitor systems; binding pose between SARS-CoV-2 Mpro + *isoacteoside/quercetin 7-o-rutinoside/ritonavir* obtained via MD simulations; and a docking list of all compounds to SARS-CoV-2 Mpro. This material is available free of charge via the Internet at <http://pubs.acs.org>.

AUTHOR INFORMATION

Corresponding Author

*Email: ngosontung@tdtu.edu.vn; duchung.pham@cchmc.org and vanvu@ntt.edu.vn

Author Contributions

STN, DHP, and VVV designed studies and wrote the manuscript. STN and NQAP performed and analyzed data. LL collected the structures of natural compounds.

Notes

The authors declare no competing financial interests.

ACKNOWLEDGMENT

This work was supported by Vietnam National Foundation for Science & Technology Development (NAFOSTED) grant #104.99-2019.57.

REFERENCES

1. Hoffmann, M.; Kleine-Weber, H.; Schroeder, S.; Krüger, N.; Herrler, T.; Erichsen, S.; Schiergens, T. S.; Herrler, G.; Wu, N.-H.; Nitsche, A.; Müller, M. A.; Drosten, C.; Pöhlmann, S., SARS-CoV-2 Cell Entry Depends on ACE2 and TMPRSS2 and Is Blocked by a Clinically Proven Protease Inhibitor. *Cell* **2020**, *181*, 1–10.
2. Fehr, A. R.; Channappanavar, R.; Perlman, S., Middle East Respiratory Syndrome: Emergence of a Pathogenic Human Coronavirus. *Annu. Rev. Med.* **2017**, *68* (1), 387-399.
3. de Wit, E.; van Doremalen, N.; Falzarano, D.; Munster, V. J., SARS and MERS: recent insights into emerging coronaviruses. *Nat. Rev. Microbiol.* **2016**, *14* (8), 523-534.
4. Lau, S. K. P.; Woo, P. C. Y.; Li, K. S. M.; Huang, Y.; Tsoi, H.-W.; Wong, B. H. L.; Wong, S. S. Y.; Leung, S.-Y.; Chan, K.-H.; Yuen, K.-Y., Severe acute respiratory syndrome coronavirus-like virus in Chinese horseshoe bats. *Proc. Natl. Acad. Sci. U.S.A* **2005**, *102* (39), 14040-14045.
5. Guan, Y.; Zheng, B. J.; He, Y. Q.; Liu, X. L.; Zhuang, Z. X.; Cheung, C. L.; Luo, S. W.; Li, P. H.; Zhang, L. J.; Guan, Y. J.; Butt, K. M.; Wong, K. L.; Chan, K. W.; Lim, W.; Shortridge, K. F.; Yuen, K. Y.; Peiris, J. S. M.; Poon, L. L. M., Isolation and Characterization of Viruses Related to the SARS Coronavirus from Animals in Southern China. *Science* **2003**, *302* (5643), 276.
6. Huang, C. L.; Wang, Y. M.; Li, X. W.; Ren, L. L.; Zhao, J. P.; Hu, Y.; Zhang, L.; Fan, G. H.; Xu, J. Y.; Gu, X. Y.; Cheng, Z. S.; Yu, T.; Xia, J. A.; Wei, Y.; Wu, W. J.; Xie, X. L.; Yin, W.; Li, H.; Liu, M.; Xiao, Y.; Gao, H.; Guo, L.; Xie, J. G.; Wang, G. F.; Jiang, R. M.; Gao, Z. C.; Jin, Q.; Wang, J. W.; Cao, B., Clinical features of patients infected with 2019 novel coronavirus in Wuhan, China. *Lancet* **2020**, *395* (10223), 497-506.
7. Wang, C.; Horby, P. W.; Hayden, F. G.; Gao, G. F., A novel coronavirus outbreak of global health concern. *Lancet* **2020**, *395* (10223), 470-473.

8. Yu Wai, C.; Chin-Pang, Y.; Kwok-Yin, W., *Prediction of the SARS-CoV-2 (2019-nCoV) 3C-like Protease (3CLpro) Structure: Virtual Screening Reveals Velpatasvir, Ledipasvir, and Other Drug Repurposing Candidates*. 2020.
9. Zhou, P.; Yang, X.-L.; Wang, X.-G.; Hu, B.; Zhang, L.; Zhang, W.; Si, H.-R.; Zhu, Y.; Li, B.; Huang, C.-L.; Chen, H.-D.; Chen, J.; Luo, Y.; Guo, H.; Jiang, R.-D.; Liu, M.-Q.; Chen, Y.; Shen, X.-R.; Wang, X.; Zheng, X.-S.; Zhao, K.; Chen, Q.-J.; Deng, F.; Liu, L.-L.; Yan, B.; Zhan, F.-X.; Wang, Y.-Y.; Xiao, G.-F.; Shi, Z.-L., A Pneumonia Outbreak Associated with a New Coronavirus of Probable Bat Origin. *Nature* **2020**, *579* (7798), 270-273.
10. Chan, J. F. W.; Yuan, S. F.; Kok, K. H.; To, K. K. W.; Chu, H.; Yang, J.; Xing, F. F.; Liu, J. L.; Yip, C. C. Y.; Poon, R. W. S.; Tsoi, H. W.; Lo, S. K. F.; Chan, K. H.; Poon, V. K. M.; Chan, W. M.; Ip, J. D.; Cai, J. P.; Cheng, V. C. C.; Chen, H. L.; Hui, C. K. M.; Yuen, K. Y., A Familial Cluster of Pneumonia Associated with the 2019 Novel Coronavirus Indicating Person-to-Person Transmission: a Study of a Family Cluster. *Lancet* **2020**, *395* (10223), 514-523.
11. WHO Coronavirus disease 2019 (COVID-19) Situation Report - 52.
12. Schoeman, D.; Fielding, B. C., Coronavirus envelope protein: current knowledge. *Virology* **2019**, *16* (1), 69.
13. Fauquet, C. M.; Fargette, D., International Committee on Taxonomy of Viruses and the 3,142 unassigned species. *Virology* **2005**, *2* (1), 64.
14. Alex, Z.; Vladimir, A.; Alexander, Z.; Bogdan, Z.; Victor, T.; Dmitry S., B.; Daniil, P.; Rim, S.; Andrey, F.; Philipp, O.; Yilin, Y.; Olga, P.; Quentin, V.; Alex, A.; Yan, I., *Potential COVID-2019 3C-like Protease Inhibitors Designed Using Generative Deep Learning Approaches*. 2020.
15. Nukoolkarn, V.; Lee, V. S.; Malaisree, M.; Aruksakulwong, O.; Hannongbua, S., Molecular Dynamic Simulations Analysis of Ritronavir and Lopinavir as SARS-CoV 3CLpro Inhibitors. *J. Theor. Biol.* **2008**, *254* (4), 861-867.
16. Efficacy and Safety of Darunavir and Cobicistat for Treatment of Pneumonia Caused by 2019-nCoV (DACO-nCoV). <https://clinicaltrials.gov/ct2/show/NCT04252274> (accessed Mar 8).
17. A Randomized, Open, Controlled Clinical Study to Evaluate the Efficacy of ASC09F and Ritonavir for 2019-nCoV Pneumonia. <https://clinicaltrials.gov/ct2/show/NCT04261270> (accessed Mar 8).
18. Marshall, G. R., Computer-Aided Drug Design. *Ann. Rev. Pharmacol. Toxicol.* **1987**, *27*, 193-213.
19. Yu, W.; MacKerell, A. D., Computer-Aided Drug Design Methods. In *Antibiotics: Methods and Protocols*, Sass, P., Ed. Springer New York: New York, NY, 2017; pp 85-106.
20. Ryde, U.; Soderhjelm, P., Ligand-Binding Affinity Estimates Supported by Quantum-Mechanical Methods. *Chem Rev* **2016**, *116* (9), 5520-5566.
21. Gehlhaar, D. K.; Verkhivker, G.; Rejto, P. A.; Fogel, D. B.; Fogel, L. J.; Freer, S. T., Docking Conformationally Flexible Small Molecules into a Protein Binding Site through Evolutionary Programming. In *Proceedings of the Fourth International Conference on Evolutionary Programming: 1-3 March 1995; San Diego*, John R, M. c. D. o. n. n. e. l. l.; Robert G, R. e. y. n. o. l. d. s.; David B, F. o. g. e. l., Eds. MIT Press: . 1995.
22. Kollman, P. A.; Massova, I.; Reyes, C.; Kuhn, B.; Huo, S.; Chong, L.; Lee, M.; Lee, T.; Duan, Y.; Wang, W.; Donini, O.; Cieplak, P.; Srinivasan, J.; Case, D. A.; Cheatham, T. E., Calculating structures and free energies of complex molecules: combining molecular mechanics and continuum models. *Acc. Chem. Res.* **2000**, *33* (12), 889-897.
23. Kuhn, B.; Kollman, P. A., Binding of a diverse set of ligands to avidin and streptavidin: an accurate quantitative prediction of their relative affinities by a combination of molecular mechanics and continuum solvent models. *J. Med. Chem.* **2000**, *43* (20), 3786-3791.
24. Wang, W.; Kollman, P. A., Computational study of protein specificity: the molecular basis of HIV-1 protease drug resistance. *Proc. Natl. Acad. Sci. USA* **2001**, *98* (26), 14937-14942.

25. Aqvist, J.; Medina, C.; Samuelsson, J.-E., A New Method for Predicting Binding Affinity in Computer-Aided Drug Design. *Protein Eng.* **1994**, 7 (3), 385-391.
26. Jones-Hertzog, D. K.; Jorgensen, W. L., Binding Affinities for Sulfonamide Inhibitors with Human Thrombin Using Monte Carlo Simulations with a Linear Response Method. *J. Med. Chem.* **1997**, 40 (10), 1539-1549.
27. Ngo, S. T.; Hung, H. M.; Nguyen, M. T., Fast and Accurate Determination of the Relative Binding Affinities of Small Compounds to HIV-1 Protease using Non-Equilibrium Work. *J. Comput. Chem.* **2016**, 37 (31), 2734-2742.
28. Zwanzig, R. W., High-temperature equation of state by a perturbation method. I. Nonpolar gases. *J. Chem. Phys.* **1954**, 22 (8), 1420-1426.
29. Beveridge, D. L.; DiCapua, F. M., Free energy via molecular simulation: applications to chemical and biomolecular systems. *Annu. Rev. Biophys. Biophys. Chem.* **1989**, 18 (1), 431-492.
30. Kirkwood, J. G., Statistical Mechanics of Fluid Mixtures. *J. Chem. Phys.* **1935**, 3 (5), 300-313.
31. Kollman, P., Free energy calculations: applications to chemical and biochemical phenomena. *Chem. Rev.* **1993**, 93 (7), 2395-2417.
32. Jarzynski, C., Equilibrium free-energy differences from nonequilibrium measurements: A master-equation approach. *Phys Rev E* **1997**, 56 (5), 5018-5035.
33. Ngo, S. T.; Nguyen, T. H.; Tung, N. T.; Nam, P. C.; Vu, K. B.; Vu, V. V., Oversampling Free Energy Perturbation Simulation in Determination of the Ligand-Binding Free Energy. *J. Comput. Chem* **2019**, n/a (n/a).
34. Jiang, W.; Roux, B., Free Energy Perturbation Hamiltonian Replica-Exchange Molecular Dynamics (FEP/H-REMD) for Absolute Ligand Binding Free Energy Calculations. *J. Chem. Theory Comput.* **2010**, 6 (9), 2559-2565.
35. Meng, Y.; Sabri Dashti, D.; Roitberg, A. E., Computing Alchemical Free Energy Differences with Hamiltonian Replica Exchange Molecular Dynamics (H-REMD) Simulations. *J. Chem. Theory Comput.* **2011**, 7 (9), 2721-2727.
36. Jiang, W.; Thirman, J.; Jo, S.; Roux, B., Reduced Free Energy Perturbation/Hamiltonian Replica Exchange Molecular Dynamics Method with Unbiased Alchemical Thermodynamic Axis. *J. Phys. Chem. B* **2018**, 122 (41), 9435-9442.
37. Christian C., G.; Georg, S., *Wuhan coronavirus 2019-nCoV – what we can find out on a structural bioinformatics level*. 2020.
38. Zhang, L.; Lin, D.; Sun, X.; Curth, U.; Drosten, C.; Sauerhering, L.; Becker, S.; Rox, K.; Hilgenfeld, R., Crystal Structure of SARS-CoV-2 Main Protease Provides a Basis for Design of Improved α -Ketoamide Inhibitors. *Science* **2020**.
39. Aliev, A. E.; Kulke, M.; Khaneja, H. S.; Chudasama, V.; Sheppard, T. D.; Lanigan, R. M., Motional Timescale Predictions by Molecular Dynamics Simulations: Case Study using Proline and Hydroxyproline Sidechain Dynamics. *Proteins: Struct., Funct., Bioinf.* **2014**, 82 (2), 195-215.
40. Wang, Y.; Xiao, J.; Suzek, T. O.; Zhang, J.; Wang, J.; Zhou, Z.; Han, L.; Karapetyan, K.; Dracheva, S.; Shoemaker, B. A.; Bolton, E.; Gindulyte, A.; Bryant, S. H., PubChem's BioAssay Database. *Nucleic Acids Res* **2012**, 40 (D1), D400-D412.
41. Wang, J.; Wang, W.; Kollman, P. A.; Case, D. A., Automatic Atom Type and Bond Type Perception in Molecular Mechanical Calculations. *J Mol Graph Model* **2006**, 25 (2), 247-260.
42. Case, D. A.; Ben-Shalom, I. Y.; Brozell, S. R.; Cerutti, D. S.; Cheatham, T. E.; Cruzeiro, I., V.W.D. ; Darden, T. A.; Duke, R. E.; Ghoreishi, D.; Gilson, M. K.; Gohlke, H.; Goetz, A. W.; Greene, D.; Harris, R.; Homeyer, N.; Huang, Y.; Izadi, S.; Kovalenko, A.; Kurtzman, T.; Lee, T. S.; LeGrand, S.; Li, P.; Lin, C.; Liu, J.; Luchko, T.; Luo, R.; Mermelstein, D. J.; Merz, K. M.; Miao, Y.; Monard, G.; Nguyen, C.; Nguyen, H.; Omelyan, I.; Onufriev, A.; Pan, F.; Qi, R.; Roe, D. R.; Roitberg, A.; Sagui, C.; Schott-Verdugo, S.; Shen, J.; Simmerling,

C. L.; Smith, J.; SalomonFerrer, R.; Swails, J.; Walker, R. C.; Wang, J.; Wei, H.; Wolf, R. M.; Wu, X.; Xiao, L.; D.M., Y.; P.A., a. K., AMBER 18. *University of California, San Francisco* **2018**.

43. Sousa da Silva, A. W.; Vranken, W. F., ACPYPE - AnteChamber PYthon Parser interfacE. *BMC Research Notes* **2012**, 5 (1), 1-8.

44. Wang, J.; Wolf, R. M.; Caldwell, J. W.; Kollman, P. A.; Case, D. A., Development and Testing of a General Amber Force Field. *J. Comput. Chem.* **2004**, 25 (9), 1157-1174.

45. Schrödinger LLC, P. *The PyMOL molecular graphics system, Versio1 1.3r1*; August, 2010.

46. Trott, O.; Olson, A. J., Improving the speed and accuracy of docking with a new scoring function, efficient optimization, and multithreading. *J. Comput. Chem.* **2010**, 31, 455-461.

47. Nguyen, N. T.; Nguyen, T. H.; Pham, T. N. H.; Huy, N. T.; Bay, M. V.; Pham, M. Q.; Nam, P. C.; Vu, V. V.; Ngo, S. T., Autodock Vina Adopts More Accurate Binding Poses but Autodock4 Forms Better Binding Affinity. *J. Chem. Inf. Model.* **2020**, 60 (1), 204-211.

48. Lee, T.-W.; Cherney, M. M.; Huitema, C.; Liu, J.; James, K. E.; Powers, J. C.; Eltis, L. D.; James, M. N. G., Crystal Structures of the Main Peptidase from the SARS Coronavirus Inhibited by a Substrate-like Aza-peptide Epoxide. *J. Mol. Biol.* **2005**, 353 (5), 1137-1151.

49. Abraham, M. J.; Murtola, T.; Schulz, R.; Páll, S.; Smith, J. C.; Hess, B.; Lindahl, E., GROMACS: High performance molecular simulations through multi-level parallelism from laptops to supercomputers. *SoftwareX* **2015**, 1-2, 19-25.

50. Ngo, S. T.; Nguyen, T. H.; Tung, N. T.; Nam, P. C.; Vu, K. B.; Vu, V. V., Oversampling Free Energy Perturbation Simulation in Determination of the Ligand-Binding Free Energy. *J. Comput. Chem* **2020**, 41 (7), 611-618.

51. Darden, T.; York, D.; Pedersen, L., Particle mesh Ewald: An N·log(N) method for Ewald sums in large systems. *J. Chem. Phys.* **1993**, 98 (12), 10089-10092.

52. Zwanzig, R. W., High-temperature equation of state by a perturbation method. I. nonpolar gases. *J. Chem. Phys.* **1954**, 22 (8), 1420-1426.

53. Bennett, C. H., Efficient estimation of free energy differences from Monte Carlo data. *J. Comput. Phys.* **1976**, 22, 245-268.

54. Laskowski, R. A.; Swindells, M. B., LigPlot+: Multiple Ligand–Protein Interaction Diagrams for Drug Discovery. *J. Chem. Inf. Model.* **2011**, 51 (10), 2778-2786.

55. S.K. Lee; I.H. Lee; H.J. Kim; G.S. Chang; J.E. Chung; No, K. T., The PreADME approach: Web-based program for rapid prediction of physico-chemical, drug absorption and drug-like properties, EuroQSAR 2002 Designing Drugs and Crop Protectants: Processes, Problems and Solutions. Blackwell Publishing: Malden, MA, 2003; pp. 418-420. <http://dx.doi.org/10.1002/cphc.201701384>.

56. Nguyen-Vo, T.-H.; Le, T.; Pham, D.; Nguyen, T.; Le, P.; Nguyen, A.; Nguyen, T.; Nguyen, T.-N.; Nguyen, V.; Do, H.; Trinh, K.; Duong, H. T.; Le, L., VIETHERB: A Database for Vietnamese Herbal Species. *J. Chem. Inf. Model.* **2019**, 59 (1), 1-9.

57. Mai, B. K.; Viet, M. H.; Li, M. S., Top-Leads for Swine Influenza A/H1N1 Virus Revealed by Steered Molecular Dynamics Approach. *J. Chem. Inf. Model.* **2010**, 50 (12), 2236-2247.

58. Jarzynski, C., Nonequilibrium Equality for Free Energy Differences. *Phys Rev Lett* **1997**, 78 (14), 2690-2693.

59. Park, S.; Schulten, K., Calculating Potentials of Mean Force from Steered Molecular Dynamics Simulations. *J. Chem. Phys.* **2004**, 120 (13), 5946-5961.

60. Cao, B.; Wang, Y.; Wen, D.; Liu, W.; Wang, J.; Fan, G.; Ruan, L.; Song, B.; Cai, Y.; Wei, M.; Li, X.; Xia, J.; Chen, N.; Xiang, J.; Yu, T.; Bai, T.; Xie, X.; Zhang, L.; Li, C.; Yuan, Y.; Chen, H.; Li, H.; Huang, H.; Tu, S.; Gong, F.; Liu, Y.; Wei, Y.; Dong, C.; Zhou, F.; Gu, X.; Xu, J.; Liu, Z.; Zhang, Y.; Li, H.; Shang, L.; Wang, K.; Li, K.; Zhou, X.; Dong, X.; Qu, Z.; Lu, S.; Hu, X.; Ruan, S.; Luo, S.; Wu, J.; Peng, L.; Cheng, F.; Pan, L.; Zou, J.; Jia, C.; Wang, J.; Liu, X.; Wang, S.; Wu, X.; Ge, Q.; He, J.; Zhan, H.; Qiu, F.; Guo, L.; Huang, C.; Jaki, T.; Hayden,

F. G.; Horby, P. W.; Zhang, D.; Wang, C., A Trial of Lopinavir–Ritonavir in Adults Hospitalized with Severe Covid-19. *N Engl J Med* **2020**.

61. Homeyer, N.; Stoll, F.; Hillisch, A.; Gohlke, H., Binding Free Energy Calculations for Lead Optimization: Assessment of Their Accuracy in an Industrial Drug Design Context. *J. Chem. Theory Comput.* **2014**, *10* (8), 3331-3344.

62. Nascimento, É. C. M.; Oliva, M.; Świderek, K.; Martins, J. B. L.; Andrés, J., Binding Analysis of Some Classical Acetylcholinesterase Inhibitors: Insights for a Rational Design Using Free Energy Perturbation Method Calculations with QM/MM MD Simulations. *J. Chem. Inf. Model.* **2017**, *57* (4), 958-976.

63. Ngo, S. T.; Fang, S.-T.; Huang, S.-H.; Chou, C.-L.; Huy, P. D. Q.; Li, M. S.; Chen, Y.-C., Anti-Arrhythmic Medication Propafenone a Potential Drug for Alzheimer's Disease Inhibiting Aggregation of A β : *In Silico* and *In Vitro* Studies. *J. Chem. Inf. Model.* **2016**, *56* (7), 1344-1356.

64. Ciordia, M.; Pérez-Benito, L.; Delgado, F.; Trabanco, A. A.; Tresadern, G., Application of Free Energy Perturbation for the Design of BACE1 Inhibitors. *J. Chem. Inf. Model.* **2016**, *56* (9), 1856-1871.

65. Tran, P.-T.; Hoang, V.-H.; Lee, J.; Hien, T. T. T.; Tung, N. T.; Ngo, S. T., In vitro and in silico determination of glutaminy cyclase inhibitors. *RSC Adv* **2019**, *9* (51), 29619-29627.

66. Sakakibara, I.; Katsuhara, T.; Ikeya, Y.; Hayashi, K.; Mitsunashi, H., Cannabisin A, an aryl-naphthalene lignanamide from fruits of *Cannabis sativa*. *Phytochemistry* **1991**, *30* (9), 3013-3016.